Microwave realization of quasi-one-dimensional systems with correlated disorder

O. Dietz,[1,*] U. Kuhl,[1,2,†] H.-J. Stöckmann,[1] N. M. Makarov,[3] and F. M. Izrailev[4]

[1]*Fachbereich Physik, Philipps-Universität Marburg, Renthof 5, D-35032 Marburg, Germany*

[2]*Laboratoire de Physique de la Matière Condensée, CNRS UMR 6622, Université de Nice Sophia-Antipolis, F-06108 Nice, France*

[3]*Instituto de Ciencias, Universidad Autónoma de Puebla, Priv. 17 Norte No 3417, Col. San Miguel Hueyotlipan, Puebla, Puebla, 72050, Mexico*

[4]*Instituto de Física, Universidad Autónoma de Puebla, Apartado Postal J-48, Puebla, Puebla, 72570, Mexico*

(Received 3 December 2010; revised manuscript received 3 February 2011; published 12 April 2011)

A microwave setup for mode-resolved transport measurement in quasi-one-dimensional (quasi-1D) structures is presented. We will demonstrate a technique for direct measurement of the Green's function of the system. With its help we will investigate quasi-1D structures with various types of disorder. We will focus on stratified structures, i.e., structures that are homogeneous perpendicular to the direction of wave propagation. In this case the interaction between different channels is absent, so wave propagation occurs individually in each open channel. We will apply analytical results developed in the theory of one-dimensional (1D) disordered models in order to explain main features of the transport. The main focus will be selective transport due to long-range correlations in the disorder. In our setup, we can intentionally introduce correlations by changing the positions of periodically spaced brass bars of finite thickness. Because of the equivalence of the stationary Schrödinger equation and the Helmholtz equation, the result can be directly applied to selective electron transport in nanowires, nanostripes, and superlattices.

DOI: 10.1103/PhysRevB.83.134203 PACS number(s): 72.15.Rn, 42.25.Bs, 42.70.Qs

I. INTRODUCTION

Because of progress in nano- and materials science, the investigation of (electron) wave propagation in periodic one-dimensional (1D) systems has recently attracted growing attention (see, e.g., Ref. 1 and references therein). Systems of particular interest are metamaterials or stacked layer structures, as well as superlattices. One of the important problems that is still far from being completely understood is the role of disorder due to fluctuations in the width of layers or due to variations in the material parameters, such as the dielectric constant, magnetic permeability, or barrier height (for electrons).[2–14] This disorder was seen mainly as an unwanted side effect in experimental realization.[12] But with enhanced ability to control these features, disorder itself becomes an interesting candidate for targeted manipulation of transport properties. In particular, the correlations in the disorder may exhibit unusual features. One of the earliest findings was that short-range correlations can inhibit localization in low-dimensional systems.[15,16]

Later it was shown, both theoretically[17–25] and experimentally,[26–29] that specific long-range correlations can even be used to significantly enhance or suppress the wave localization in any desired windows of frequency. Recent analytical studies extended the theoretical predictions from purely 1D models to quasi-one-dimensional (quasi-1D) randomly stratified structures,[23,30] as well as to random, periodic-on-average stacked systems with bilayer unit cells.[31–34] These studies provide the application of correlated disorder to photonic crystals, metamaterials, and layered structures, e.g., semiconductor superlattices.

In this paper we explore the validity and applicability of the theoretical results by studying the microwave transmission through a quasi-1D waveguide open on both ends. It was shown in Ref. 35 that the transport properties can be effectively studied by measurement of the Green's function, up to a factor describing the antenna properties. This method can be considered an essential tool to analyze the experimental data. It allows us to test experimentally the analytical predictions from Ref. 35 in open waveguides with and without disorder. Furthermore, we extend the experimental confirmation of selective transport to quasi-1D systems that emerge because of long-range correlations. Many studies on 1D systems with correlated disorder involve hundreds of scatterers.[16,26,27] In presented experiments only 26 scatterers are used. We demonstrate that this small number is already sufficient to reveal the predicted effect of correlated disorder.

II. EXPERIMENTAL SETUP AND BASIC EQUATIONS

In our study we use an experimental setup that allows us to measure microwave transport through a multimode metallic-wall waveguide with an internal structure of different kinds (see Fig. 1). The input (transmitting) and output (receiving) antennas are plugged into the waveguide via slides that can be shifted stepwise by two motors. The absorbers are placed on both ends of the waveguide, in order to reduce the reflection from the ends, i.e., to consider the setup as a *finite waveguide with open ends*. The values of the height h, width w, and distance between the antennas—the effective length L of the waveguide—meet the conditions

$$h \ll w \ll L \tag{2.1}$$

that are important for a proper theoretical analysis.

In an empty rectangular waveguide, the electromagnetic field can be separated into two components of different polarization: the TM polarization with transverse magnetic field and the TE polarization with transverse electric field.[36] In our experiments, all measurements are performed below the cut-off frequency $\nu_{\text{cut}} = c/2h \approx 18.75$ GHz. In this case only the lowest TE component, having the electric field stretched

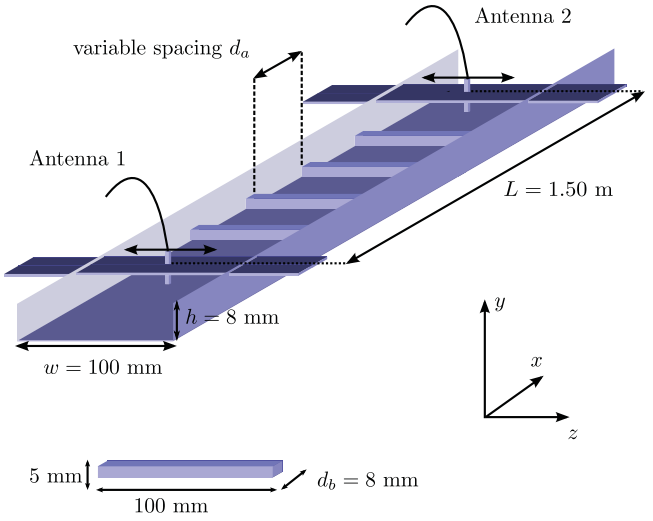

FIG. 1. (Color online) Not-to-scale sketch of experimental setup with top plate removed. Brass-bar inlays can be freely placed inside the waveguide. Number of bars varies according to spacing d_a. Antennas shown here with parts of the top plate can be moved separately along the z direction. Distance along the x axis between antennas is $L = 1.50$ m; total waveguide length is 2.38 m. Absorbers at the ends of the waveguide are omitted.

along the y axis and the magnetic field in the xz plane (see the coordinate system in Fig. 1), can propagate. Therefore, our experimental setup within the frequency interval $\nu < \nu_{\text{cut}}$ and with the conditions in Eq. (2.1) can be considered as a quasi-1D open-strip structure, occupying the region

$$0 \leqslant x \leqslant L, \quad 0 \leqslant z \leqslant w. \tag{2.2}$$

In order to develop a proper theory for our model, we treat the input antenna 1 in the xz plane as a point source, while the output antenna 2 is an observation point. As is known, the electric field of a point source is determined by the retarded Green's function $\mathcal{G}(|x - x'|; z, z')$. In Ref. 35 it was shown that for the correct analysis of transport one has to take into account the influence of coupling between the antennas and the waveguide. As a result, the Green's function for the empty waveguide in the normal-mode representation reads

$$\mathcal{G}(|x - x'|; z, z') = \sum_{n=1}^{N_w} A_n \sin\left(\frac{\pi n z}{w}\right) \sin\left(\frac{\pi n z'}{w}\right) \times \frac{\exp(ik_n|x - x'|)}{ik_n w}. \tag{2.3}$$

Here we introduced the factor A_n, which effectively describes the coupling between the antennas and normal modes labeled by index n. In our experiment this factor A_n is regarded as a fitting parameter. Without antenna coupling ($A_n = 1$), Eq. (2.3) coincides with the Green's function of the two-dimensional Helmholtz equation complemented by the Dirichlet boundary conditions at metallic walls of the waveguide.

The quantities $\pi n/w$ and k_n are, respectively, the discrete values of transverse, k_z, and longitudinal, k_x, wave numbers:

$$k_n = \sqrt{k^2 - (\pi n/w)^2} = \frac{2\pi}{c}\sqrt{\nu^2 - (n\nu_c)^2}, \quad n = 1,2,3,\ldots,N_w. \tag{2.4}$$

Here $k = 2\pi\nu/c$ is the total wave number for the electromagnetic wave of frequency ν. For the modeling of electron quasi-1D structures (such as nanowires and nanostripes), the wave number k should be regarded as the Fermi wave number within the isotropic Fermi-liquid model.

The total number N_w of propagating waveguide modes (for which k_n is real) is determined by the integer part $[\![\ldots]\!]$ of the mode parameter $kw/\pi = \nu/\nu_c$:

$$N_w = [\![kw/\pi]\!] = [\![\nu/\nu_c]\!]. \tag{2.5}$$

Correspondingly, the sum in Eq. (2.3) runs only over the propagating modes with $n \leqslant N_w$ and ignores the contribution of evanescent modes for which $n > N_w$. Indeed, for evanescent modes the values of k_n are purely imaginary; therefore, they do not contribute to the transport. The critical frequency ν_c,

$$\nu_c = c/2w, \tag{2.6}$$

below which there are only evanescent modes ($kw/\pi < 1$, i.e., $N_w = 0$), is called the cut-off frequency. Evidently, there is no transport for $\nu < \nu_c$. Note that here ν_c is the cut-off frequency for the first mode with $n = 1$. The cut-off frequency $\nu_c^{(n)}$ for each higher mode with index n is given by $\nu_c^{(n)} = n\nu_c$.

III. SCATTERING MATRIX

It is suitable to define the scattering matrix S_{nm} for the whole waveguide ($|x - x'| = L$) as the twofold sine-Fourier transform:

$$S_{nm} = \frac{2}{w}\int_0^w dz\, dz' \sin\left(\frac{\pi n z}{w}\right) \sin\left(\frac{\pi m z'}{w}\right) \mathcal{G}(L; z, z'). \tag{3.1}$$

One can see that in accordance with Eq. (2.3), the scattering matrix for the empty quasi-1D waveguide [Eq. (2.2)] is diagonal in the mode representation. In this case the S matrix is proportional to the Green's function for free 1D propagation with the wave number k_n:

$$S_{nm} = A_n \frac{\exp(ik_n L)}{2ik_n} \Theta(N_w - n)\delta_{nm}. \tag{3.2}$$

Here $\Theta(x)$ stands for the Heaviside unit-step function, where $\Theta(x < 0) = 0$ and $\Theta(x \geqslant 0) = 1$. The result [Eq. (3.2)] is quite natural, since in an empty waveguide there are no transitions between the normal modes. Therefore, the transport through any channel can be considered independently of other channels.

Below we call the elements S_{nm} of the scattering matrix [Eq. (3.1)] scattering amplitudes. Then, the scattering probability T_{nm} from mode n to mode m, the mode-transport coefficient T_n (for the scattering of a given nth "incoming"

mode into all "outgoing" modes), and the total transport coefficient T are naturally defined as follows:

$$T_{nm} = |S_{nm}|^2, \quad T_n = \sum_{m=1}^{N_w} T_{nm}, \quad T = \sum_{n=1}^{N_w} T_n. \qquad (3.3)$$

One should stress that although the above definitions of T_{nm}, T_n, and T correspond to the standard ones known in the theory of transport through quasi-1D disordered structures (e.g., see Ref. 37), here the physical meaning of all these quantities is different. Indeed, the expression for the scattering matrix S_{nm} is originated from the single-particle Green's function, not from the Kubo formula, which is based on the two-particle Green's function. The price for this simplification can be directly seen from Eq. (3.2), which has a divergence at values of $k_n = 0$. Therefore, the transmission coefficients [Eq. (3.3)] cannot be normalized. On the other hand, there is no divergence in the standard expressions for scattering matrices. However, our point is that this somewhat new definition of the scattering matrix, based on the mode representation of the Green's function, has an advantage when we consider setups similar to the one in our experiment. In spite of the absence of rigorous expressions for the localization length developed in connection with this type of scattering matrix, in the following we show that the knowledge of theoretical results obtained for 1D disordered models very much helps us to understand the transport properties of the experimental setup.

For the experimental data analysis, the continuous Fourier transform [Eq. (3.1)] is replaced by its discrete counterpart, allowing us to compute S_{nm} from $\mathcal{G}(L;z,z')$ measured for different positions z and z' of input and output antennas. A typical measurement series with the starting points $z = z' =$ 5 mm and step size 10 mm yields 10^2 individual measurements. An example of the transmission spectrum obtained in one measurement is shown in Fig. 2. It should be kept in mind that in our experiment the total transport coefficient T is always less than 1, since the antennas are not perfectly coupled to the waveguide. Furthermore, at both ends about half the energy escapes toward the open ends. The amount of energy lost is not accessible in the present setup. Moreover, the absorption inside the waveguide reduces the value of T further. Practically, in our experiment the total transport coefficient T never exceeds the value $T = 0.17$.

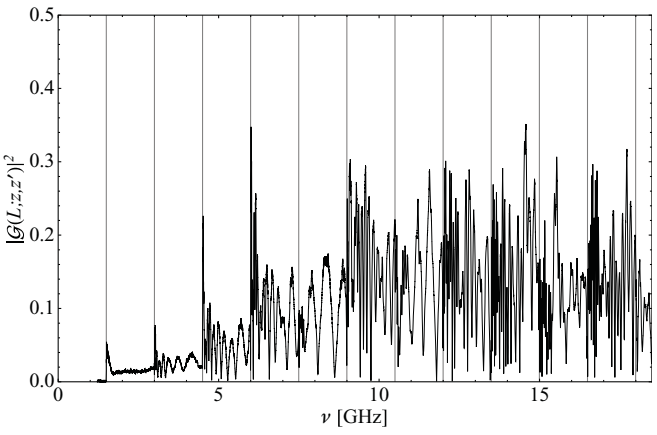

FIG. 2. Transmission spectrum $|\mathcal{G}(L;z,z')|^2$ through the empty waveguide for fixed antenna position $z = z' = 55$ mm. Vertical lines show the cut-off frequencies $\nu_c^{(n)}$ for different modes.

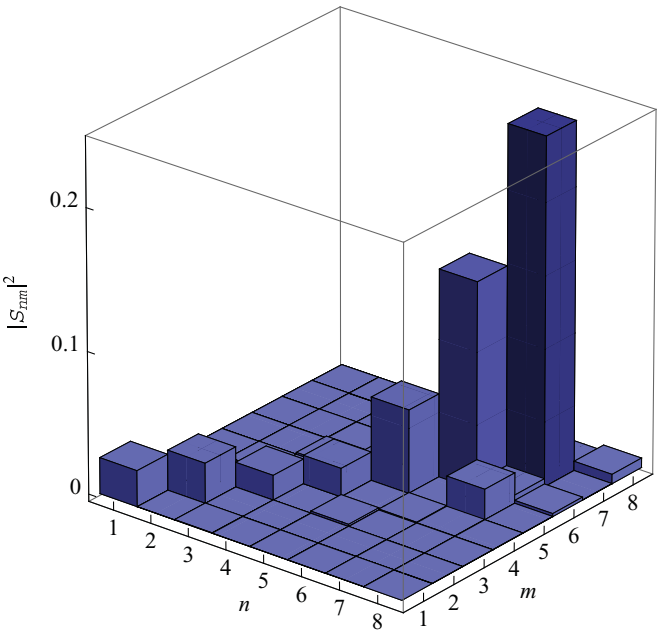

FIG. 3. (Color online) Modulus square of the scattering matrix elements $T_{nm} = |S_{nm}|^2$ at $\nu = 11$ GHz with seven propagating modes.

The Fourier transform [Eq. (3.1)] can be performed for every single frequency ν in the spectra, yielding the scattering matrix S_{nm} as a function of ν. An example of the scattering probability $T_{nm} = |S_{nm}|^2$ for an empty waveguide and fixed value $\nu = 11$ GHz is shown in Fig. 3. At this frequency there are seven propagating modes. Since there are no scatterers in the waveguide, there should be no transitions between different propagating modes; therefore, the matrix T_{nm} is expected to be diagonal in accordance with Eq. (3.2). Experimentally, the total contribution of the off-diagonal elements in comparison with that of diagonal elements is found to be always less than 5% (typically much smaller). The main source of these off-diagonal terms is the perturbation caused by antennas. We always observe that the highest propagating mode gives the main contribution to the transport, as in Fig. 3, where the term $|S_{77}|^2$ is the largest one. This fact is in complete correspondence with the expectation from the theoretical predictions discussed in the next section.

IV. EMPTY WAVEGUIDE

Let us analyze the transport through various modes as a function of the wave frequency. As an example, the measured frequency dependence of the mode-transport coefficient [Eq. (3.3)] for the third $T_3(\nu)$ and the fourth $T_4(\nu)$ modes is depicted in Fig. 4 by solid curves. There are several interesting features in this figure. First of all, there is a pronounced spike in $T_3(\nu)$ at the cut-off frequency $\nu_c^{(3)} = 4.5$ GHz, at which the third mode opens and starts to propagate. The experimental value of $\nu_c^{(3)}$ coincides very well with the theoretical prediction, $\nu_c^{(3)} = 3c/2w$ [see Eq. (2.6) and comments below it]. Above this critical value the coefficient T_3 decreases for increasing frequency.

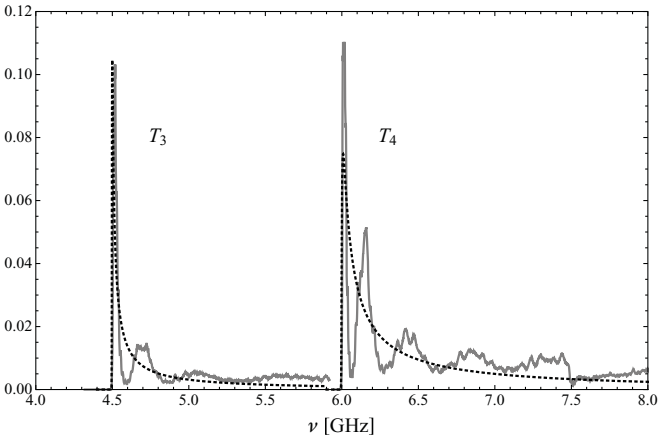

FIG. 4. Mode propagation for the third and fourth modes through the empty waveguide (solid line) compared to the theoretical prediction of Eq. (4.1) (dotted line). Here $|A_3|^2 = 30$ and $\mathrm{Im}\, k = 0.03$ for the third mode, and $|A_4|^2 = 146$ and $\mathrm{Im}\, k = 0.06$ for the fourth one.

The frequency dependence of $T_4(\nu)$ looks quite similar to that of $T_3(\nu)$, apart from the shift of the spectrum by the value $\nu_c = c/2w = 1.5$ GHz. This is because propagation of the fourth mode emerges above the cut-off frequency $\nu_c^{(4)} = 4c/2w = 6.0$ GHz. In general, all mode-transport coefficients $T_n(\nu)$ have somewhat similar frequency dependencies. Namely, they manifest the corresponding spikes at the corresponding cut-off values, $\nu_c^{(n)} = nc/2w$, and decrease with further frequency increase.

In order to understand such specific frequency dependence of the coefficients $T_n(\nu)$, one has to use Eqs. (3.2) and (2.4). Since in an empty waveguide all propagating modes are independent of each other, the mode-transport coefficient reads

$$T_n(\nu) = |S_{nn}|^2 = \frac{|A_n|^2}{4|k_n|^2}\Theta(N_w - n)$$

$$= \frac{c^2|A_n|^2}{16\pi^2\left(\nu^2 - n^2\nu_c^2\right)}\Theta(\nu - n\nu_c). \qquad (4.1)$$

One can easily achieve a nice correspondence of this theoretical result to the experimental data by a simple fit of the factor A_n. To do this, we must also take into account an evident assumption that the wave number k (i.e., the frequency ν) has a small imaginary part $\mathrm{Im}\, k$ (or $\mathrm{Im}\, \nu$), which emerges because of an absorption in the waveguide.

Typically, the absorption is frequency dependent, but in the analysis it is sufficient to treat it as a constant for each mode, i.e., to regard $\mathrm{Im}\, k$ as a function of the mode index n only. In Fig. 4 the theoretical expression (4.1) is displayed by dotted curves. Note, however, that the fast oscillations clearly seen in the experimental curves are not described by our theory. These oscillations are caused by multiple wave reflections from the waveguide ends (occurring because of nonperfect absorbers) and from the antennas.

The frequency dependence experimentally observed for the coefficient $T_n(\nu)$ is explained by the presence of the squared modulus of longitudinal wave number k_n in the denominator of Eq. (4.1). Apart from the frequency dependence, this term, $|k_n|^2 = \frac{4\pi^2}{c^2}(\nu^2 - n^2\nu_c^2)$, provides the global dependence of $T_n(\nu)$ on the mode index n. One can see that at fixed frequency ν the higher the mode index n, the larger the coefficient $T_n(\nu)$. That is why the highest propagating mode with $n = N_w$ always gives the main contribution to the total transport coefficient T, especially in the vicinity of its cut-off, $\nu_c^{(N_w)} = N_w c/2w$. This effect is displayed in Fig. 3.

V. PERIODIC STRUCTURE

The features of the empty waveguide discussed above were explored as a necessary precondition for our further analysis. As a second step, we studied a periodic structure without any disorder. To this end, the brass bars of thickness $d_b = 8$ mm measured along the x axis were inserted into the waveguide as is shown in Fig. 1. The constant spacing d_a between neighboring bars was chosen as $d_a = 17$ mm and $d_a = 32$ mm for two different realizations, yielding a period $d = d_a + d_b = 25$ mm for the first realization with 42 bars, and $d = 40$ mm for the second one with 26 bars. The measurements were performed as before, giving rise to the scattering matrix S_{nm} of the periodic setup. Both periodic structures gave similar results; therefore, in what follows, we restrict the discussion to the second case only. It would be interesting to investigate the behavior of the bands and the correlation gaps with decreasing number of scatterers N_d, but this is beyond the scope of the present paper.

Since the periodic structure is arranged along the wave propagation (along the x axis) and the bars are homogeneous along the z axis, the propagating modes remain independent as in the empty waveguide. Indeed, the scattering matrix [Eq. (3.1)] was experimentally found to be diagonal within the same accuracy as before. As a consequence, the spectrum of the mode-transport coefficient $T_n(\nu) = |S_{nn}|^2$ looks similar for all propagating modes, provided the shift of spectrum by particular cut-off frequencies, $\nu_c^{(n)} = nc/2w$, is done. This means that $T_n(\nu)$ is convenient to represent as a function of the corresponding longitudinal wave number $k_x = k_n$ [see Eq. (2.4)]. Figure 5(a) shows the semilogarithmic experimental plot of the mode-transport coefficient $T_3(k_3)$ for the third propagating mode. One can clearly see a band structure in the dependence $T_3(k_3)$, as is expected for a periodic arrangement. Note that the experimental transmission in the gaps is smaller than in the bands over several orders of magnitude.

From the physical point of view, our setup with periodic filling of brass bars represents a set of N_w independent 1D periodic arrays of two alternating a and b layers. Note, however, that each unit (a,b) cell of every nth array has a quite complicated structure. While the first a layer is a trivially homogeneous air spacing of thickness d_a with the wave number k_n, the second b layer of thickness d_b is not homogeneous along the y axis. Indeed, since the height (5 mm) of the brass bar is smaller than the waveguide height ($h = 8$ mm), there is an air slot between the metallic bar and the waveguide top plate (see Fig. 1). For this reason, in our analysis we shall characterize the b layers by the wave number $k_b = n_b k_n$, thus introducing an *effective* refractive index n_b that should be fixed by the experimental data. In this way, in order to describe the transmission band structure for every nth array of bilayers (for every nth propagating mode), we

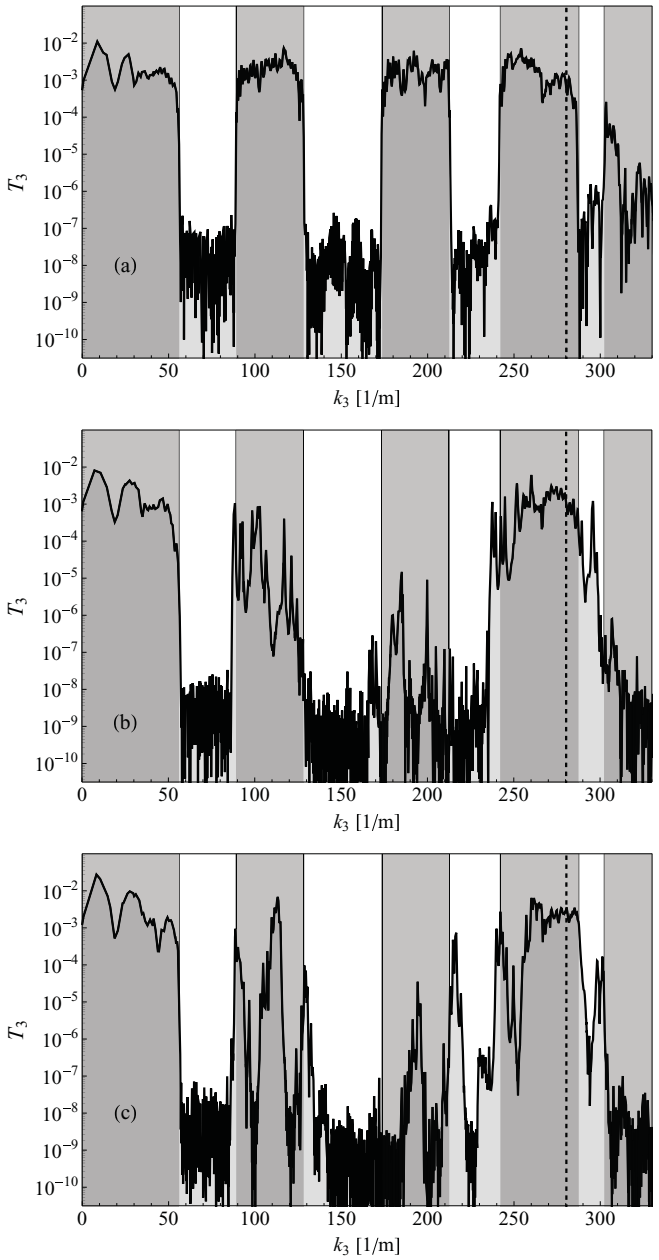

FIG. 5. Band structure for (a) periodic, (b) white-noise, and (c) correlated-disorder arrangements with $\langle d_a(j)\rangle = d_a = 32$ mm. Shaded regions indicate the bands restricted by phenomenologically obtained band edges (vertical lines). Dashed vertical line indicates the Fabry-Pérot resonance (see Sec. VI A).

employ the effective Kronig-Penney model with the common dispersion relation for the Bloch wave number κ (see, e.g., Refs. 1 and 38):

$$\cos(\kappa d) = \cos(k_n d_a)\cos(n_b k_n d_b) - \alpha_+ \sin(k_n d_a)\sin(n_b k_n d_b). \quad (5.1)$$

For the standard bilayer models the factor α_+ is the arithmetic average of the impedance ratio and its inverse value: $\alpha_+ = (Z_a/Z_b + Z_b/Z_a)/2$. Since the impedance Z_b of b layers is unknown for our system, the factor α_+ is regarded as

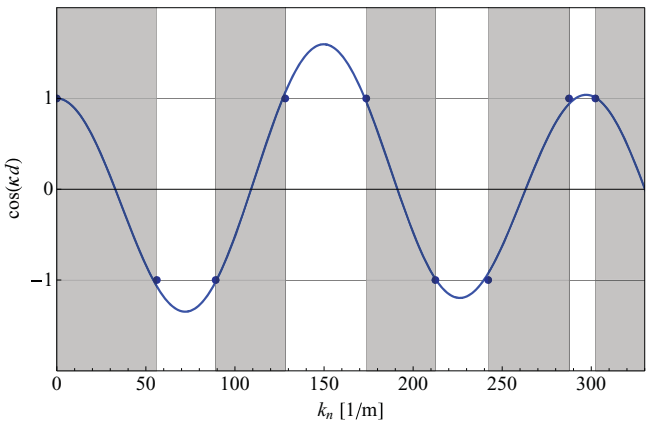

FIG. 6. (Color online) The right-hand side of the dispersion relation [Eq. (5.1)] (solid line) for the best fit of the parameters. The spacing is $d_a = 32$ mm with fitting parameters $\alpha_+ = 1.6$ and $n_b = 1.42$. Dark dots correspond to the band edges extracted from Fig. 5(a).

the second fitting parameter. Note that $\alpha_+ = 1$ for the case of two basic layers a and b that are optically matched ($Z_a = Z_b$).

The solution of Eq. (5.1) gives the Bloch wave number $\kappa = \kappa(k_n)$ as a function of the mode wave number k_n (i.e., as a function of the wave frequency ν and the mode index n). The real values of κ are achieved for k_n where $|\cos(\kappa d)| < 1$, thus resulting in the emergence of spectral transmission bands. Otherwise, for k_n where $|\cos(\kappa d)| > 1$, the Bloch wave number κ turns out to be imaginary, leading to the emergence of spectral gaps. The dispersion relation [Eq. (5.1)] gives the band edges at the points where $\cos(\kappa d) = \pm 1$.

As a first step, we manually extracted the positions of the band edges from the measured spectrum of the coefficient $T_n(\nu) = |S_{nn}|^2$ (see vertical lines in Fig. 5 for these positions). Then we fitted the dispersion relation [Eq. (5.1)] by changing the values of α_+ and n_b, and keeping the points of its right-hand side that intersected with the horizontal lines $\cos(\kappa d) = \pm 1$, in correspondence with the found band edges. The result is displayed in Fig.6 for $\alpha_+ = 1.6$ and $n_b = 1.42$. The dark dots in the figure show the extracted band edges.

VI. POSITIONAL DISORDER

In order to study the effect of disorder, we shifted each brass bar by a random value along the waveguide length (the x axis), keeping the average distance between the bars constant. Since the disorder is a function of the x coordinate only, the propagating modes remain independent as in the arrangements considered above.[23,30] In such a manner, we can consider every nth channel as an independent 1D array of two alternating a (air spacing) and b (brass bar) layers. Theoretically, the positional disorder is incorporated via the random thickness of a layers only:

$$d_a(j) = d_a + \varrho_a(j), \qquad \langle d_a(j)\rangle = d_a, \quad (6.1)$$

while the thickness d_b of b layers is constant. The integer $j = 1,2,3,\ldots,N_d$, where $N_d = [\![L/d]\!]$, enumerates the unit (a,b) cells; d_a is the average thickness of the a layer; and $\varrho_a(j)$ stands for small random variations. Note that in the absence

of disorder ($\varrho_a = 0$), the set of 1D bilayer arrays represents the periodic structure with the period $d = d_a + d_b$ that was considered in the previous section.

The random sequence $\varrho_a(j)$ is statistically homogeneous with the zero average and given variance σ_a^2:

$$\langle \varrho_a(j) \rangle = 0\,, \qquad \langle \varrho_a^2(j) \rangle = \sigma_a^2\,. \tag{6.2}$$

The binary correlator is defined by

$$\langle \varrho_a(j)\varrho_a(j') \rangle = \sigma_a^2 K_a(j - j')\,. \tag{6.3}$$

Averaging $\langle \ldots \rangle$ is performed over the whole array of layers or over different ensembles, which are assumed to be equivalent. As one can see, the two-point correlator $K_a(j - j')$ is normalized to unity: $K_a(0) = 1$.

If the positional disorder is weak ($k_a^2\sigma_a^2 \ll 1$), all transport properties are determined entirely by the randomness power spectrum $\mathcal{K}_a(k)$,

$$\mathcal{K}_a(k) = 1 + 2\sum_{r=1}^{\infty} K_a(r)\cos(kr), \tag{6.4a}$$

$$K_a(r) = \frac{1}{\pi}\int_0^{\pi} dk \mathcal{K}_a(k)\cos(kr). \tag{6.4b}$$

Since the correlator $K_a(r)$ is a real and even function of the difference $r = j - j'$ between cell indices, its Fourier transform $\mathcal{K}_a(k)$ is a real and even function of the dimensionless wave number k. According to the Wiener-Khinchin theorem, the power spectrum $\mathcal{K}_a(k)$ is non-negative for *any* real sequence $\varrho_a(j)$.

The transport through any 1D disordered structure is governed by the phenomenon of Anderson localization (see, e.g., Ref. 39). Its principal concept is that all transport characteristics depend only on the ratio between the system length L and localization length $L_{\rm loc}$. Thus, localization length is the key quantity that controls the transport in a 1D geometry. The analytical expression for localization length in the periodic-on-average model with bilayer structure was derived in Ref. 31. Specifically, the case of weak disorder in the thickness of only one kind of layer was analyzed, which is close to our experimental setup.

However, our model is essentially quasi-1D. On the other hand, in Refs. 23 and 30 it was shown that in quasi-1D waveguides with random stratification *along* the propagation, each of the (independent) modes can be associated with their own length $L_{\rm loc}(k_n)$. The latter can be obtained by direct substitution of specific mode characteristics into the general expression for the localization length of 1D random structures. Applying the results from Refs. 23, 30, and 31, one can readily get the following expression for the inverse localization length, associated with the nth propagating mode of our setup:

$$L_{\rm loc}^{-1}(k_n) = \frac{\alpha_-^2 k_n^2 \sigma_a^2}{2d\sin^2(\kappa d)}\mathcal{K}_a(2\kappa d)\sin^2(n_b k_n d_b). \tag{6.5}$$

Here α_-^2 is the so-called mismatching factor. For standard bilayer models α_- is related to α_+ in the dispersion relation [Eq. (5.1)] by the equality $\alpha_+^2 - \alpha_-^2 = 1$. Therefore, for the perfect matching where $\alpha_+ = 1$, we have $\alpha_- = 0$, resulting in a divergence of the localization length, $L_{\rm loc} = \infty$. Since for our system $\alpha_+ = 1.6$, the mismatching factor is $\alpha_-^2 = 1.56$.

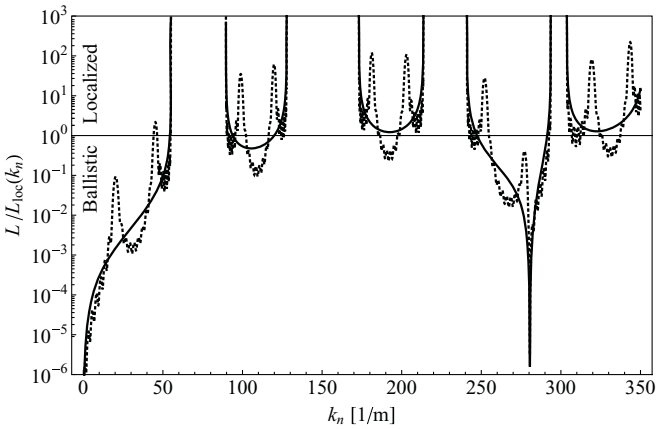

FIG. 7. Ratio $L/L_{\rm loc}(k_n)$ formed by Eq. (6.5) for white-noise disorder (solid curve) and for correlated disorder (dotted curve). Parameters are $d_a = 32$ mm, $\sigma_a = 2.21$ mm, $\alpha_-^2 = 1.56$. Horizontal line indicates the equality $L = L_{\rm loc}(k_n)$.

Note that Eq. (6.5) is a particular case of a more general expression derived in Ref. 32 for the case of both a and b positional disorders (when thicknesses of both a and b layers are randomly perturbed).

A. White-noise disorder

In Fig. 7 the inverse localization length $L_{\rm loc}^{-1}(k_n)$ of the nth propagating mode, measured in units of the waveguide length $L = 1.5$ m, is plotted against k_n. The 26 displacements $\varrho_a(j)$ were drawn randomly from the interval -5 mm to 5 mm, while the variance was constrained to $\sigma_a^2 = 4.9$ mm^2. The ratio of σ_a and the spacing d_a is about 7%.

Now we start with the discussion of experimental data for the case of uncorrelated (white-noise) disorder. In this case the binary correlator is $K_a(j - j') = \delta_{jj'}$, and consequently, the power spectrum is constant: $\mathcal{K}_a(k) = 1$. The corresponding ratio $L/L_{\rm loc}(k_n)$ is represented in Fig. 7 by a solid curve. One can see that within the first spectral band, the inverse localization length monotonously increases from zero to infinity depending on k_n. Within any other Bloch band the mode-localization length $L_{\rm loc}(k_n)$ vanishes at the band edges (where $\kappa d = 0, \pi$) because of the term $\sin^2(\kappa d)$ in the denominator of Eq. (6.5).

It is important that the mode-localization length $L_{\rm loc}(k_n)$ exhibits the Fabry-Pérot resonances associated with multiple wave reflections inside every b layer from its interfaces. As is known, the resonances appear when the constant width d_b is equal to an integer multiple of half of the wavelength inside the layer:

$$k_n = \pi s/n_b d_b\,, \qquad s = 1,\ 2,\ 3, \ldots\,. \tag{6.6}$$

At the resonances the factor $\sin^2(n_b k_n d_b)$ in Eq. (6.5) vanishes, resulting in resonance divergence of the localization length and, consequently, in suppression of the localization (the nth mode becomes fully transparent). Remarkably, the Fabry-Pérot resonance should be quite broad, since it is caused by the vanishing of a smooth trigonometric function. This effect was analyzed both theoretically and experimentally in Refs. 33 and 34. Since in our experimental setup $n_b = 1.42$ and $d_b = 8$ mm, the first ($s = 1$) Fabry-Pérot resonance is expected at

$k_n = 280.5\ \mathrm{m}^{-1}$, and this is what is observed in the fourth transmission band in Fig. 7.

In accordance with single-parameter scaling, there are only two transport regimes in the 1D Anderson localization: the ballistic ($L \ll L_{\mathrm{loc}}$) and localized ($L_{\mathrm{loc}} \ll L$) regimes. In the ballistic regime a sample is practically transparent, and in the localized regime a 1D disordered structure almost perfectly reflects classical or quantum waves.

In Fig. 7 the horizontal straight line $L/L_{\mathrm{loc}}(k_n) = 1$ separates the upper region, $L/L_{\mathrm{loc}}(k_n) > 1$ (where the nth propagating mode is localized, and therefore closed), from the lower one, $L/L_{\mathrm{loc}}(k_n) < 1$ (where the nth propagating mode is transparent). As one can see from Fig. 7, in our experiments the first and fourth spectral bands should be almost completely transparent. Note that the transparency of the first band is due to a very weak influence of the disorder, while the transparency of the fourth band is caused by the broad Fabry-Pérot resonance.

The predicted features of the system are clearly displayed in Fig. 5 for the experimentally measured mode-transport coefficient $T_3(k_3)$. A comparison of Figs. 5(a) and 5(b) shows that the introduced disorder does not reduce transmission in the first band, where $k_n < 50\ \mathrm{m}^{-1}$. In the fourth band, between $240\ \mathrm{m}^{-1}$ and $290\ \mathrm{m}^{-1}$, again there is only a weak influence of disorder. Only in the second, third, and fifth bands does the compositional disorder reduce the mode transport by 2–3 orders of magnitude.

B. Correlated disorder

As one can see from Eq. (6.5), the inverse localization length $L_{\mathrm{loc}}^{-1}(k_n)$ follows the profile of the power spectrum $\mathcal{K}_a(2\kappa d)$. This fact is of special interest in view of experimental realizations of positional disorder with specific long-range correlations. In particular, one can artificially construct an array of random bilayers with a power spectrum that vanishes abruptly within prescribed intervals of the mode wave number k_n, resulting in the divergence of the mode-localization length. Thus, by proper design of the positional disorder, one can create quasi-1D bilayer structure with a *selective* mode transmission $T_n(k_n)$ dependent on the frequency ν.

To do this, we perturbed all periodically spaced, $N_d = 26$, brass bars by random values $\varrho_a(j)$ ($j = 1,2,3,\ldots,N_d$) correlated in such a way that the power spectrum $\mathcal{K}_a(2\kappa d)$ is zero everywhere, except for narrow regions around $\kappa d/\pi = 0.3$ and 0.7.

We can solve the problem of generating the random sequences with prescribed short- or long-range correlators by employing a widely used convolution method originally proposed by Rice.[40] The details of various applications of this method can be found in Refs. 17–19, 21–23, 26, 27, 30, and 41–48. With the use of this method, the resulting curve for $\mathcal{K}_a(2\kappa d)$ has the form shown in Fig. 8. For comparison, the power spectrum for an uncorrelated random sequence is also shown. The inverse dimensionless localization length $L/L_{\mathrm{loc}}(k_n)$ that corresponds to the specified correlated disorder is depicted in Fig. 7 by the dotted curve. In accordance with this curve, one should expect the appearance of correlation gaps, i.e., additional gaps due to correlated disorder (namely, one correlation gap in the first band and two in the second and third transmission bands). In the first band the first possible correlation gap at $k_n \approx 25\ \mathrm{m}^{-1}$ remains in the ballistic regime and cannot be observed. The same happens in the fourth band, where only the first correlation gap can be observed. Because of the overlap with the Fabry-Pérot resonance, the second correlation gap is shifted to the ballistic regime.

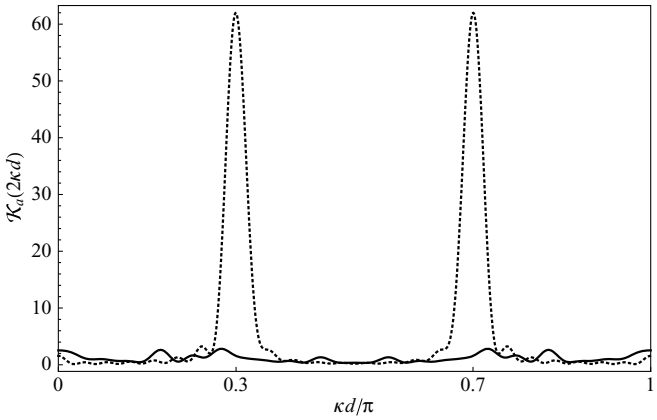

FIG. 8. Power spectrum $\mathcal{K}_a(2\kappa d)$ versus dimensionless Bloch phase $\kappa d/\pi$ for correlated (dotted curve) and uncorrelated (solid curve) random sequences. The factor $\mathcal{K}_a(2\kappa d)$ is calculated from Eq. (6.4), taking only the first 13 terms in the sum that corresponds to an arrangement with $N_d = [\![L/d]\!] = 26$ unit (a,b) cells with $\langle d_a(j)\rangle = d_a = 32$ mm.

Figure 5(c) shows the mode transmission through the correlated random arrangement. Globally, the spectral structure looks similar to that for the uncorrelated random setup. Indeed, we can see that the transport decreases with increase of k_n, with an exception of the fourth band containing the Fabry-Pérot resonance. In the first band the mode-transport coefficient $T_n(k_n)$ is comparable to that for both regular and uncorrelated random setup: Figs. 5(a) and 5(b). This is because in this band the localization length is larger than the system size: $L \ll L_{\mathrm{loc}}(k_n)$. Only in the region of the correlation gap at $k_n = 40\ \mathrm{m}^{-1}$ does the localization length shrink, such that $L_{\mathrm{loc}}(k_n) \approx L$, resulting in a very weak but recognizable correlation gap. This correlation gap is an interesting special case, because it is in the regime intermediate between ballistic and localized.

The second band exhibits two correlation gaps that are clearly seen, in spite of the fact that in this band the transport is reduced by two orders of magnitude. In the third spectral band, at about $k_n = 200\ \mathrm{m}^{-1}$, the transport already decreased to noise level. However, in the fourth band containing the Fabry-Pérot resonance, the transport is quite large and comparable to that for the regular arrangement—apart from one correlation gap. Finally, within the fifth band the mode-transport coefficient is reduced by randomness so strongly that it is not possible to reveal any difference between correlated and uncorrelated disorder. All these properties are in complete agreement with the predictions provided by our theoretical model.

In order to compare the effects of uncorrelated and correlated disorder in more detail, we present Fig. 9, which illustrates the second and fourth spectral bands of the mode-transport coefficient $T_n(k_n)$ for the third propagating mode. The expected positions of the correlation gaps at $\kappa d/\pi = 0.3, 0.7$

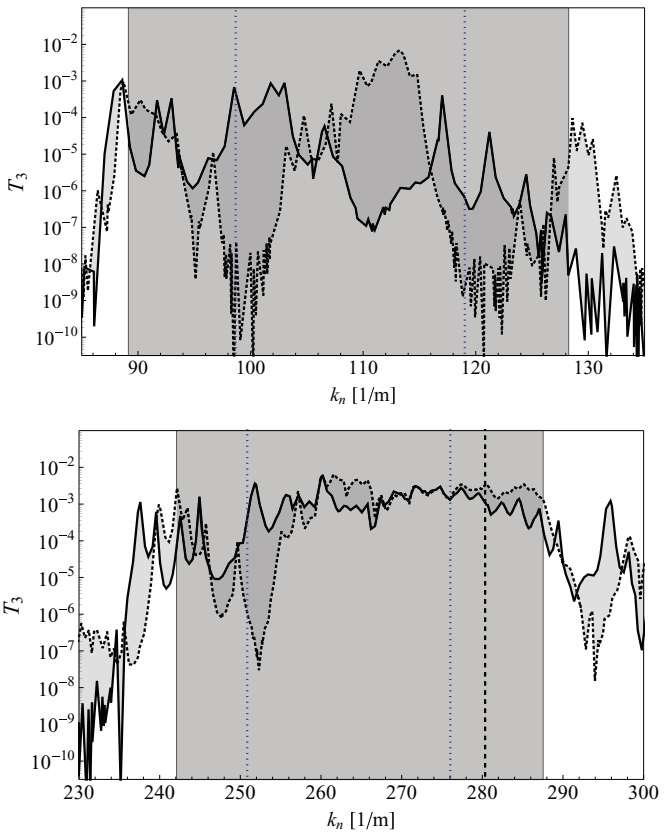

FIG. 9. (Color online) Comparison of the mode-transport coefficient through uncorrelated (solid curve) and correlated (dotted curve) random arrangements. Upper figure shows the second band; lower figure presents the fourth (Fabry-Pérot) band. Vertical dotted line indicates expected correlation gaps for $\kappa d/\pi = 0.3,\ 0.7$. Vertical dashed line indicates the position of the Fabry-Pérot resonance at $k_n = 280.5\ \mathrm{m}^{-1}$.

are indicated by vertical dotted lines, and the position of the Fabry-Pérot resonance is given by the vertical dashed line.

In the second spectral band (see upper part of Fig. 9), the correlation gaps are easily recognized, showing the variation of the amplitude over five orders of magnitude. There is good agreement between the theoretically predicted and experimentally found positions of these correlation gaps. Between the correlation gaps, i.e., in the vicinity of $k_x = 110\ \mathrm{m}^{-1}$, the mode-transport coefficient for correlated disorder is two orders of magnitude higher than for uncorrelated disorder. Again, this is not surprising, since the power spectrum $\mathcal{K}_a(k) \approx 1$ for uncorrelated disorder, whereas in the case of correlated disorder it is close to zero outside the correlation gaps. Remember that the mode-localization length [Eq. (6.5)] tends to infinity as $\mathcal{K}_a(k) \to 0$.

In the fourth spectral band containing the Fabry-Pérot resonance (lower part of Fig. 9), only the first correlation gap is found. The second correlation gap is at a short distance from the Fabry-Pérot resonance and therefore is suppressed. Indeed, here because of the resonance, the mode-localization length is still quite large, $L \ll L_{\mathrm{loc}}(k_n)$, in order to contribute to transmission of the waveguide of finite length (see also Fig. 7). Only for the first correlation gap does the mode-localization length turn out to be sufficiently small, $L_{\mathrm{loc}}(k_n) \ll L$, to observe this gap. Note that for white-noise disorder the fourth band is almost fully transparent, exclusively because of the Fabry-Pérot resonance. Nonetheless, the specific correlations in the positional disorder of the brass bars can induce a correlation gap, provided that the distance between the resonance and the corresponding maximum of the power spectrum $\mathcal{K}_a(2\kappa d)$ is sufficiently long.

Finally, we would like to stress that all peculiar effects discussed above are experimentally observed for a quite short quasi-1D system, with as few as $N_d = 26$ brass bars. This fact confirms the expectation that the analytical expression for the localization length, formally obtained for infinite systems, is actually applicable for real experimental situations with a relatively small number of scatterers.

VII. CONCLUSIONS

We studied transport through a quasi-1D microwave waveguide with periodic and randomized scattering potentials. The potentials were stratified, i.e., homogeneous along the width of the waveguide. In this case the propagation of waves occurs independently along each open channel, thus allowing one to apply the theory of 1D transport to any partial channel and make conclusions about both partial and total transmission.

In the experimental setup the incoming and outgoing waves are induced by pointlike antennas. Therefore, one of the problems was to understand the influence of the coupling of antennas to the waveguides, as well as the role of reflection from the antennas and the open ends. Also, the effect of absorption in the walls influenced the transport characteristics. We have tried to incorporate all these effects in our phenomenological theory aiming to explain the observed data.

Main attention was paid to selective transport due to long-range correlations in the disorder. We generated the disorder by intentionally shifting the position of bulk scatterers. In order to quantify our experimental setup, we started with the case of an open waveguide without any scatterers. In this case we confirmed that the coupling between various channels due to antennas is small and can be neglected when compared to the theoretical predictions. Then we studied scattering through the waveguide with periodically inserted scatterers chosen in the form of finite-thickness brass bars. With such an arrangement, the transmission spectrum was found to have a band structure, as expected. However, in order to analytically describe the structure of the spectrum, one must create a phenomenological model that properly corresponds to the experimental setup.

The specific problem we encountered was that the periodic brass bars inserted in the waveguide cannot simply be considered as finite-thickness barriers with certain refractive indices. They are made of metal, and in order to allow propagation they have a finite height that is less than the vertical dimension of the waveguide. In this case it impractical to rigorously create a relatively simple and adequate theoretical model, and instead we decided to use the standard dispersion relation known in the theory of 1D models, by introducing two fitting parameters. In this way we were able to give an analytical expression for the positions of transmission bands and spectral gaps. This expression helped us describe another experiment, in which

the positions of brass bars were slightly perturbed, both in a random manner and with specific long-range correlations.

For the case of uncorrelated disorder, we obtained experimental data that can be described by an analytical expression for the localization length. For any kind of correlation, the corresponding expression was derived in Refs. 23, 30–32, and one of our interests was to check how well our experimental data correspond to the predictions of the theory. It should be stressed that this problem is far from trivial, since the expression for the localization length was developed for the infinite number of scatterers and for weak disorder. In our case, the number of scattering bars $N_d = 26$ was relatively small, and many other experimental imperfections (absorption, nonperfect coupling, etc.) are not taken into account in the expression for localization length. However, the experimental data were found to correspond well with our expectations following from the theory. In particular, a quite unusual effect of Fabry-Pérot resonances was observed in experimental data, which is fully explained by the theory.

The Fabry-Pérot resonances were predicted to play a specific role in the transport (see discussion in Refs. 33 and 34). Namely, if one such resonance emerges inside the transmission band, the transmission coefficient turns out to be very large, compared with the bands without such a resonance. The nontrivial point is that the resonance effect occurs not only for a specific frequency, but in a large interval of frequencies inside the band. In our experiment we have clearly observed the Fabry-Pérot resonance in the fourth band. The transport in this band would be negligible otherwise.

Another specific interest was to check whether in our setup with a finite number of brass-bar scatterers one can observe the effect of long-range correlations embedded intentionally in the positions of bars. According to the theory, with specific long-range correlations one can construct such potentials for which the localization length (obtained in the first-order perturbation theory) diverges (or is very small) in finite windows of frequency. In these windows one can observe either strongly enhanced or strongly suppressed transport, compared to the white-noise disorder case. In order to observe experimentally the effect of suppression of the transmission, we created disordered perturbations of the positions of brass bars, in accordance with theoretical expressions for long-range correlations. Remarkably, our experimental data clearly manifest the emergence of new gaps inside the transmission bands, in good correspondence with analytical expressions. In particular, these gaps were found to arise at the positions that were predicted theoretically.

ACKNOWLEDGMENTS

The authors are thankful to Timur Tudorovskiy for fruitful discussions. O.D., U.K., H.-J.S., and F.M.I acknowledge support from the Deutsche Forschungsgemeinschaft within research group 760, "Scattering Systems with Complex Dynamics." F.M.I acknowledges additional support from Vicerrectoría de Investigación y Estudios de Posgrado Grant No. EXC08-G of the Benemérita Universidad Autónoma de Puebla (Mexico).

*otto.dietz@physik.uni-marburg.de
†ulrich.kuhl@unice.fr

[1] *Wave Propagation: From Electrons to Photonic Crystals and Left-Handed Materials*, edited by P. Markoš and C. M. Soukoulis (Princeton University, Princeton, NJ, 2008).
[2] V. Baluni and J. Willemsen, Phys. Rev. A **31**, 3358 (1985).
[3] A. R. McGurn, K. T. Christensen, F. M. Mueller, and A. A. Maradudin, Phys. Rev. B **47**, 13120 (1993).
[4] D. R. Smith, W. J. Padilla, D. C. Vier, S. C. Nemat-Nasser, and S. Schultz, Phys. Rev. Lett. **84**, 4184 (2000).
[5] R. A. Shelby, D. R. Smith, and S. Schultz, Science **292**, 77 (2001).
[6] C. G. Parazzoli, R. B. Greegor, K. Li, B. E. C. Koltenbah, and M. Tanielian, Phys. Rev. Lett. **90**, 107401 (2003).
[7] A. Esmailpour, M. Esmaeilzadeh, E. Faizabadi, P. Carpena, and M. R. R. Tabar, Phys. Rev. B **74**, 024206 (2006).
[8] Y. Dong and X. Zhang, Phys. Lett. A **359**, 542 (2006).
[9] D. Nau, A. Schönhardt, C. Bauer, A. Christ, T. Zentgraf, J. Kuhl, M. W. Klein, and H. Giessen, Phys. Rev. Lett. **98**, 133902 (2007).
[10] I. V. Ponomarev, M. Schwab, G. Dasbach, M. Bayer, T. L. Reinecke, J. P. Reithmaier, and A. Forchel, Phys. Rev. B **75**, 205434 (2007).
[11] A. A. Asatryan, L. C. Botten, M. A. Byrne, V. D. Freilikher, S. A. Gredeskul, I. V. Shadrivov, R. C. McPhedran, and Y. S. Kivshar, Phys. Rev. Lett. **99**, 193902 (2007).
[12] F. M. Izrailev, N. M. Makarov, and E. J. Torres-Herrera, Physica B **405**, 3022 (2010).
[13] A. A. Asatryan, S. A. Gredeskul, L. C. Botten, M. A. Byrne, V. D. Freilikher, I. V. Shadrivov, R. C. McPhedran, and Y. S. Kivshar, Phys. Rev. B **81**, 075124 (2010).
[14] D. Mogilevtsev, F. A. Pinheiro, R. R. dos Santos, S. B. Cavalcanti, and L. E. Oliveira, Phys. Rev. B **82**, 081105(R) (2010).
[15] D. H. Dunlap, H.-L. Wu, and P. W. Phillips, Phys. Rev. Lett. **65**, 88 (1990).
[16] V. Bellani, E. Diez, R. Hey, L. Toni, L. Tarricone, G. B. Parravicini, F. Domínguez-Adame, and R. Gomez-Alcala, Phys. Rev. Lett. **82**, 2159 (1999).
[17] F. M. Izrailev and A. A. Krokhin, Phys. Rev. Lett. **82**, 4062 (1999).
[18] A. Krokhin and F. Izrailev, Ann. Phys. (Leipzig) **8**, 153 (1999).
[19] F. M. Izrailev, A. A. Krokhin, and S. E. Ulloa, Phys. Rev. B **63**, 041102(R) (2001).
[20] J. C. Hernández Herrejón, F. M. Izrailev, and L. Tessieri, Physica E **40**, 3137 (2008).
[21] F. M. Izrailev and N. M. Makarov, Opt. Lett. **26**, 1604 (2001).
[22] F. M. Izrailev and N. M. Makarov, Phys. Rev. B **67**, 113402 (2003).
[23] F. M. Izrailev and N. M. Makarov, J. Phys. A **38**, 10613 (2005).
[24] E. Diez, F. Izrailev, A. Krokhin, and A. Rodriguez, Phys. Rev. B **78**, 035118 (2008).
[25] F. M. Izrailev, Mesoscopic Physics in Complex Media 01006 (2010).
[26] U. Kuhl, F. M. Izrailev, A. A. Krokhin, and H.-J. Stöckmann, Appl. Phys. Lett. **77**, 633 (2000).

[27]U. Kuhl, F. M. Izrailev, and A. A. Krokhin, Phys. Rev. Lett. **100**, 126402 (2008).
[28]O. Dietz, U. Kuhl, H.-J. Stöckmann, F. M. Izrailev, and N. M. Makarov, Mesoscopic Physics in Complex Media 03010 (2010).
[29]U. Kuhl, Mesoscopic Physics in Complex Media 01017 (2010).
[30]F. M. Izrailev and N. M. Makarov, Appl. Phys. Lett. **84**, 5150 (2004).
[31]N. M. Makarov, F. M. Izrailev, and G. Luna-Acosta, in *Proceedings of the 6th International Kharkov Symposium on Physics and Engineering of Microwaves, Millimeter, and Submillimeter Waves and Workshop on Terahertz Technologies* (Kharkov, 2007), Vol. 1, p. 140.
[32]F. M. Izrailev and N. M. Makarov, Phys. Rev. Lett. **102**, 203901 (2009).
[33]G. A. Luna-Acosta, F. M. Izrailev, N. M. Makarov, U. Kuhl, and H.-J. Stöckmann, Phys. Rev. B **80**, 115112 (2009).
[34]G. A. Luna-Acosta and N. M. Makarov, Ann. Phys. (NY) **18**, 887 (2009).
[35]T. Tudorovskiy, R. Höhmann, U. Kuhl, and H.-J. Stöckmann, J. Phys. A **41**, 275101 (2008).
[36]J. D. Jackson, *Classical Electrodynamics* (Wiley, New York, 1962).
[37]C. W. J. Beenakker, Rev. Mod. Phys. **69**, 731 (1997).
[38]R. de L. Kronig and W. G. Penney, Proc. R. Soc. A **130**, 499 (1931).
[39]I. M. Lifshitz, S. Gredeskul, and L. Pastur, *Introduction to the Theory of Disordered Systems* (Wiley, New York, 1988).
[40]S. O. Rice, Bell Systems Tech. J. **23**, 282 (1944); in *Selected Papers on Noise and Stochastic Processes*, edited by N. Wax (Dover, New York, 1954), p. 180.
[41]C. S. West and K. A. O'Donnell, J. Opt. Soc. Am. A **12**, 390 (1995).
[42]A. Czirók, R. N. Mantegna, S. Havlin, and H. E. Stanley, Phys. Rev. E **52**, 446 (1995).
[43]H. A. Makse, S. Havlin, M. Schwartz, and H. E. Stanley, Phys. Rev. E **53**, 5445 (1996).
[44]A. H. Romero and J. M. Sancho, J. Comput. Phys. **156**, 1 (1999).
[45]J. García-Ojalvo and J. Sancho, *Noise in Spatially Extended Systems* (Springer-Verlag, New York, 1999).
[46]R. Cakir, P. Grigolini, and A. A. Krokhin, Phys. Rev. E **74**, 021108 (2006).
[47]F. M. Izrailev, A. A. Krokhin, N. M. Makarov, and O. V. Usatenko, Phys. Rev. E **76**, 027701 (2007).
[48]S. S. Apostolov, F. M. Izrailev, N. M. Makarov, Z. A. Mayzelis, S. S. Melnyk, and O. V. Usatenko, J. Phys. A **41**, 093901 (2008).